THE JOURNAL OF PHYSICAL CHEMISTRY B

Article

pubs.acs.org/JPCB

A Structural Study of an Organogel Investigated by Small-Angle Neutron Scattering and Synchrotron Small-Angle X-ray Scattering

Hiroyuki Takeno,*[,†] Akiko Maehara,[†] Daisuke Yamaguchi,[‡] and Satoshi Koizumi[‡]

[†]Department of Chemistry and Chemical Biology, Faculty of Engineering, Gunma University, Kiryu, Gunma 376-8515, Japan

[‡]Japan Atomic Energy Agency, Tokai, Ibaragi 319-1195, Japan

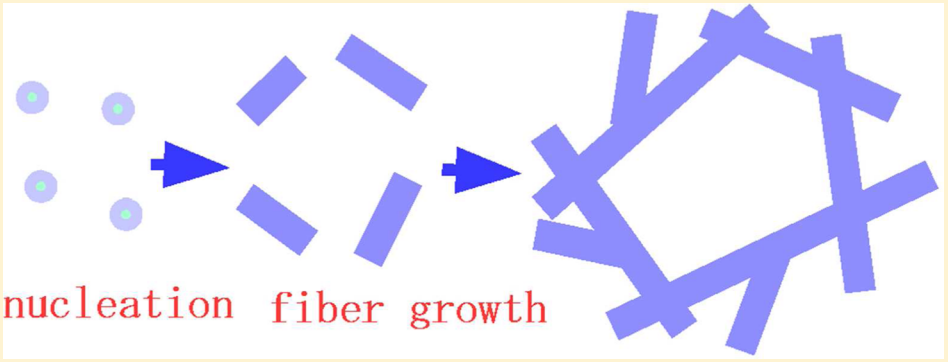

ABSTRACT: We investigated structures of 12-hydroxystearic acid (12-HSA) gels in a wide temperature range from the gel to the sol states and the gelation process by means of small-angle neutron scattering (SANS) and time-resolved synchrotron small-angle X-ray scattering (SAXS), respectively. The SANS result shows that the size of the cross section of the crystalline fibers in the gel was not affected much by temperature change, although the density of the fibers decreased with the increase of temperature even in the gel state. The SANS profiles at various temperatures and compositions were well reduced by the product of the volume fraction of the fiber and the square of the scattering contrast. At temperatures above the melting point of the gels obtained from differential scanning calorimeter, the gel turned into a homogeneous solution. The time-resolved small-angle X-ray scattering experiments revealed the gelation process as mentioned below. At the early stage, the scattering behavior did not show any change (induction period). The induction period was longer at higher temperatures. In the second stage, an amorphous precursor appeared as an initial structure of crystalline nucleus. In the next stage, the fiber was developed via crystalline nucleation and growth. In this stage, the fibers grew with keeping the size of the cross section (the radius of gyration $R \cong 82-84$ Å) constant, and finally, the fiber growth was arrested because of gelation.

INTRODUCTION

Some materials, which are called low-molecular weight gelators, form a three-dimensional fibril network by self-assembling in an organic solvent.[1,2] The self-assembled fibrillar networks are mainly caused by noncovalent interactions such as hydrogen bonding, van der Waals interactions, and electrostatic interactions. In many cases, the fibrillar network has crystalline or pseudocrystalline natures, and therefore, the sol−gel transition is related to the melting of the crystalline fibers as well as to the crystalline polymer gels.[1,3] In the case of the polymer gel, some researchers showed that the gel does not melt to a homogeneous solution but does melt to a solution containing aggregates at high temperatures.[4,5] In the case of the crystalline low-molecular mass organogels (LMOG), the structure above the sol−gel transition temperature seems to be uncertain. Moreover, there may be some differences between the crystalline polymer gels and the crystalline LMOG. In the former case, the crystallites mainly work as the junction points, and there exist a lot of amorphous chains connected with the junction points.[6] On the other hand, in the latter case, it seems to be believed that the whole fibers are crystalline. So far, numerous studies on structures of the organogels have been conducted at room temperature.[7−9] Usually, the shape or the size of the fibers largely depends on the kind of the solvent even if the same gelator was used.[10] Terech et al. investigated the structure of 12-hydroxystearic acid (12-HSA), which is well-known as one of the organogelators, in a variety of solvents by using small-angle neutron scattering (SANS). They showed that the gelator molecules in the gel packed in a monocrystalline form, where hydrogen bonding between hydroxyl groups along the fiber axis and head-to-head contacts between carboxylic acid groups are formed.[11] Thus, though many studies have so far been devoted to structures of LMOG at room temperature, to our knowledge, few extensive studies have been conducted on the structures in the wide range from the gel to the sol states. On the other hand, not only structures in an equilibrium state (or in a steady state) but also the self-assembling process of LMOG is an important subject in

Received: January 26, 2012
Revised: June 7, 2012
Published: June 9, 2012

dx.doi.org/10.1021/jp3008514 | J. Phys. Chem. B 2012, 116, 7739−7745

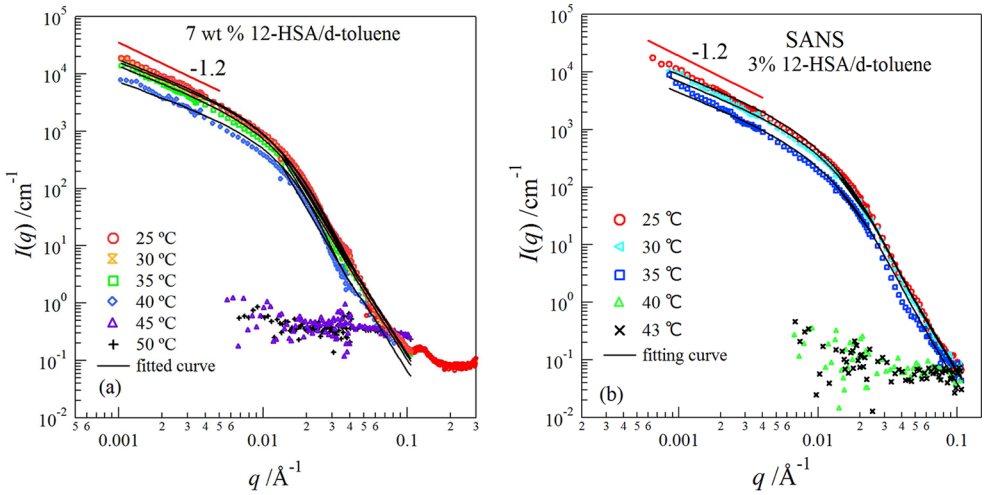

Figure 1. SANS profiles at various temperatures for (a) 7 wt % 12-HSA gel and (b) 3 wt % 12-HSA gel . The solid lines represent the fitted curves.

an understanding of the gelation mechanism. On the whole, as the structural evolution of LMOG is so fast, it is usually difficult to experimentally pursue it. Time-resolved synchrotron small-angle X-ray scattering (SAXS) measurements are a very powerful technique to overcome it. The technique enables us to measure the scattering intensity in the exposure time of ca. 1 s or less.

In this study, we are concerned with two subjects: (1) structure of LMOG in the wide temperature range from gel to sol states and (2) the structural development during the gelation process. We performed SANS measurements for the former purpose and the in-situ synchrotron time-resolved SAXS measurements for the latter purpose for a mixture of 12-HSA and an organic solvent.

EXPERIMENTAL SECTION

Material. 12-HSA sample was purchased from Wako Chemical Co. and was purified by using a mixture with a composition of hexane/ethyl acetate = 90/10 wt/wt % as a solvent and by changing the temperature.[12] After the 12-HSA with a known concentration was dissolved in toluene by increasing the temperature, the sample was put at the ambient temperature to prepare the gel. A transparent gel is formed in toluene.

SANS. Deuterated toluene was used as the solvent to obtain the larger scattering contrast. SANS measurements were carried out using the SANS-J-II instrument at the JRR-3 M research reactor of the Japan Atomic Energy Agency (JAEA) in Tokai, Japan. The neutron beam was monochromatized with a velocity selector to have a wavelength λ of 6.56 Å and $\Delta\lambda/\lambda$ = 0.11, where $\Delta\lambda$ is the full width at half-maximum (fwhm). To cover a wide q range ($q = 4\pi \sin(\theta/2)/\lambda$, where θ is the scattering angle), that is, to obtain information on structure over a wide range of the spatial scale, the measurements were conducted under three conditions: at detector position of (1) D = 2.5 m, (2) D = 10 m, and (3) D = 10 m with a focusing SANS[13] which enables us to obtain scattering data in a very low q range by using focusing biconcave lenses made of MgF_2 compounds and a high-resolution photomultiplier. Furthermore, a wide-angle neutron-scattering experiment was performed at 25 °C for 7 wt % 12-HSA gel. The scattered intensity was detected with a two-dimensional ^{3}He position-sensitive detector. After the detected scattering intensity was corrected for detector sensitivity, electric noise, and solid angle, it was circularly averaged to obtain the scattering profile as a function of q. Furthermore, the scattering profile was corrected for empty cell scattering, sample thickness, and transmission and then was reduced to absolute units (cm^{-1}) using a porous aluminum plate as a secondary standard.

SAXS. Synchrotron SAXS measurements were performed at the beamline 15A (BL15A) of the Photon Factory at the High Energy Acceleration Research Organization in Tsukuba, Japan. The scattered X-ray with a wavelength of 1.5 Å was detected with an image intensifier coupled to a charge-coupled device (CCD) camera. The two-dimensional CCD images were circularly averaged to obtain the scattering intensity as a function of q. The scattering data were corrected for distortion of the CCD image, background scattering, electrical background, strength of incident X-ray beam, and exposure time. The sample-to-detector position was obtained using the data of collagen with a spacing of 653 Å, which was 2275 mm. The samples for the SAXS experiments were put into a borosilicate glass tube with a diameter of 1.5 mm. Time-resolved SAXS measurements were performed by using a temperature-jump cell designed for investigation of a self-assembling process. The details of the cell are described elsewhere.[14] The SAXS data were taken as a function of time after the sample was quenched from a sol state into a gel state.

Differential Scanning Calorimetry (DSC). Melting points of the gels were obtained with a differential scanning calorimeter, Perkin-Elmer DSC7 calorimeter, at a heating rate of 3 °C min^{-1}. Indium and cyclohexane were used to calibrate the temperature scale. Samples for the measurements were sealed with aluminum cells. We estimated the melting point of the gel from the peak point of the DSC traces.

RESULTS

Temperature Dependence of Gel Structures. Figure 1 presents SANS profiles at various temperatures for the 7 wt % 12-HSA/toluene gel (a) and for 3 wt % 12-HSA/toluene gel (b). The profile for the 7 wt % 12-HSA/toluene gel at 25 °C, which was measured in wider scattering angles, has a peak at q = 0.125 $Å^{-1}$. The peak corresponds to (001) reflection according to previous studies.[11,15] The peak position slightly shifts toward smaller q relative to that of the powder, although the peak position for the gels in other solvents is almost the

dx.doi.org/10.1021/jp3008514 | J. Phys. Chem. B 2012, 116, 7739−7745

same as that of the powder as reported in the previous study.[15] The SANS profiles in the gel state for all the compositions had almost the same shape in the log−log plot and showed the behavior of $I(q) \sim q^{-1.2}$ in the small q region. The exponent is slightly larger than that expected from the scattering behavior of rod particles ($I(q) \sim q^{-1}$) in the small q range. The slight increase of the exponent may reflect ramification of the fibers. The profiles for both compositions show that the scattering intensity gradually decreased with an increase of temperature until a certain temperature and drastically decreased at temperatures higher than it. The former result suggests that a part of the fibers gradually melted with an increase of temperature even in the gel state. The drastic decrease in the scattering intensity was seen at $T \geq 45$ °C for 7 wt % 12-HSA gel and at $T \geq 40$ °C for 3 wt % 12-HSA gel. This behavior can be ascribed to the transition from gel into sol. The result is consistent with the DSC result, for example, the endothermic peaks for 7 wt % and 3 wt % 12-HSA/toluene gels were observed at 42.4 °C and at 38.3 °C, respectively. The scattering profiles were almost independent of q in the high-temperature range. The result suggests that the mixture was completely homogeneous above the melting temperature obtained from DSC measurements. The same trend was observed for the 1 wt % 12-HSA gel.

Here, let us discuss the structural analysis of the gel. Generally, the scattering intensity contains intra- and interparticle scattering contribution. The latter effect usually depends upon the concentration of the particles. In our systems, the shape of the SANS profiles was not affected by the composition of the gelator indicating that the contribution of the interparticle scattering is negligibly small. Therefore, we analyzed the SANS profiles with the form factor $P(q)$ of the randomly distributed rod particles with the height $2H$ ($2H = L$) and the diameter $2R$, which is described by[16,17]

$$P(q) = 4\int_0^{\pi/2}\left[\frac{\sin^2(qH\cos\beta)}{(qH\cos\beta)^2}\right]\left[\frac{J_1^2(qR\sin\beta)}{(qR\sin\beta)^2}\right]\sin\beta\,\mathrm{d}\beta \tag{1}$$

where β is the angle between the scattering vector q and the axis of the rod. We fitted the scattering profiles in the whole q range using the scattering function with the log-normal distribution of the cross-sectional size as follows:

$$I(q) = \int_0^\infty (\Delta\rho)^2 V^2 N(R) P(q)\,\mathrm{d}R \tag{2}$$

with

$$N(R) = N_\nu\left(\frac{1}{R\sqrt{2\pi}\ln\sigma_g}\right)\exp[-(\ln R - \ln R_0)^2/2\ln^2\sigma_g] \tag{3}$$

where N_ν represents the number density of fibers (rod particles). R_0 and σ_g are the geometric mean and the geometric standard deviation of the distribution, respectively. $\Delta\rho$ and V represent the difference in the density of the neutron scattering length and the volume of the rod particles, respectively. Because the matrix phase is the solution of HSA in d-toluene, $\Delta\rho$ is described by

$$\Delta\rho = \rho_{HSA} - \{x_{sol,HSA}\rho_{HSA} + (1 - x_{sol,HSA})\rho_{d\text{-}tol}\} \tag{4}$$

where ρ_i is the scattering length density of the component i (i = HSA or deuterated toluene) defined by $N_A\sum b_i/\nu_i$, where N_A, b_i, and ν_i are the Avogadro number, the neutron scattering length, and the molar volume of the component i, respectively. The value of ν_i for HSA was taken from the literature.[11] $x_{sol,HSA}$ is the mole fraction of HSA in the matrix phase, and the method to evaluate it at a given temperature will be mentioned later. As a result, $\Delta\rho$ has the value of -5.60×10^{10} cm^{-2} at 25 °C. The mean radius of the rod particles with the size distribution $\langle R\rangle$ and their volume fraction ϕ_{rod} are presented as follows, respectively,

$$\langle R\rangle = \int_0^\infty RN(R)\mathrm{d}R \tag{5}$$

and

$$\phi_{rod} = \int_0^\infty (\pi R^2 2H)N(R)\mathrm{d}R \tag{6}$$

In the fitting procedure, we first calculated the form factor of rod particles with the cross-sectional size distribution $I_{calc}(q)$, and afterward, the parameters were determined to minimize $\chi = \sum\{\log[xI_{calc}(q)] - \log[I_{data}(q)]\}^2$, where x and $I_{data}(q)$ represent a prefactor and the experimental data, respectively. The solid line in Figure 1 represents the fitted curves. The result shows a good agreement between the data and the calculated curve. In this fitting analysis, we obtained values of H larger than 10 000 Å except for the case of 40 °C for 7 wt % HSA gel as shown in Figure 2. It was difficult to obtain a definite H value because the χ value in the fit did not change much in the range of sufficiently large H. This is because the scattering profiles showed the behavior of $q^{-1.2}$ even in the experimental limit ($q \sim 0.0008$ Å^{-1}). As shown in Figure 2, the parameters H and N_v correlate, that is, larger H leads to less N_v. However, as long as we use sufficiently large H, the difference in the H values does not affect the estimate of other fitting parameters. A drastic decrease in H for 7 wt % HSA gel at 40 °C near the melting point may indicate collapse of the network, and such behavior, however, was not observed for other compositions. In the case of 7 wt % HSA gel at 25 °C, $R_0 = 80$ Å and $\sigma_g = 1.5$ were obtained, which corresponds to $\langle R\rangle = 87$ Å. The cross-sectional size is close to that reported by Terech et al.[10] We present the temperature dependence of $\langle R\rangle$ and σ_g obtained from the fitted result in Figure 2b and c. Except for the neighborhood of the sol−gel transition temperature, it is shown that $\langle R\rangle$ and σ_g are almost constant against temperature variation. Furthermore, we obtained the volume fraction of the fibers ϕ_{rod} with eq 6 at various temperatures. The temperature dependence of ϕ_{rod} obtained thus is shown in Figure 3 (see open symbols). ϕ_{rod} decreased with an increase of temperature, that is, it is shown that the fibers gradually melted with the increase of temperature in the gel state. Thus, the SANS result reveals that the fiber thickness does not change, while the fiber density decreases with an increase of temperature.

In-Situ Time-Resolved SAXS. We show time evolution of the SAXS profiles for 7 wt % 12-HSA in toluene after the temperature jump (T-jump) from 50 °C (sol) to 34 °C (gel) in Figure 4. The scattering profiles did not change with elapse of time at the early stage, which corresponds to the induction period. Afterward, the scattering intensity in the small q-range increased with time, but the (001) peak was not observed in this stage. Namely, an initial structure of nucleus appeared in the regime before the crystalline nucleation stage. In the next stage, the (001) reflection peak appeared at 56.1 s, that is, nucleation took place. In the case of the T-jump to 30 °C, the appearance of the (001) peak occurred at 23.8 s. The time

dx.doi.org/10.1021/jp3008514 | J. Phys. Chem. B 2012, 116, 7739−7745

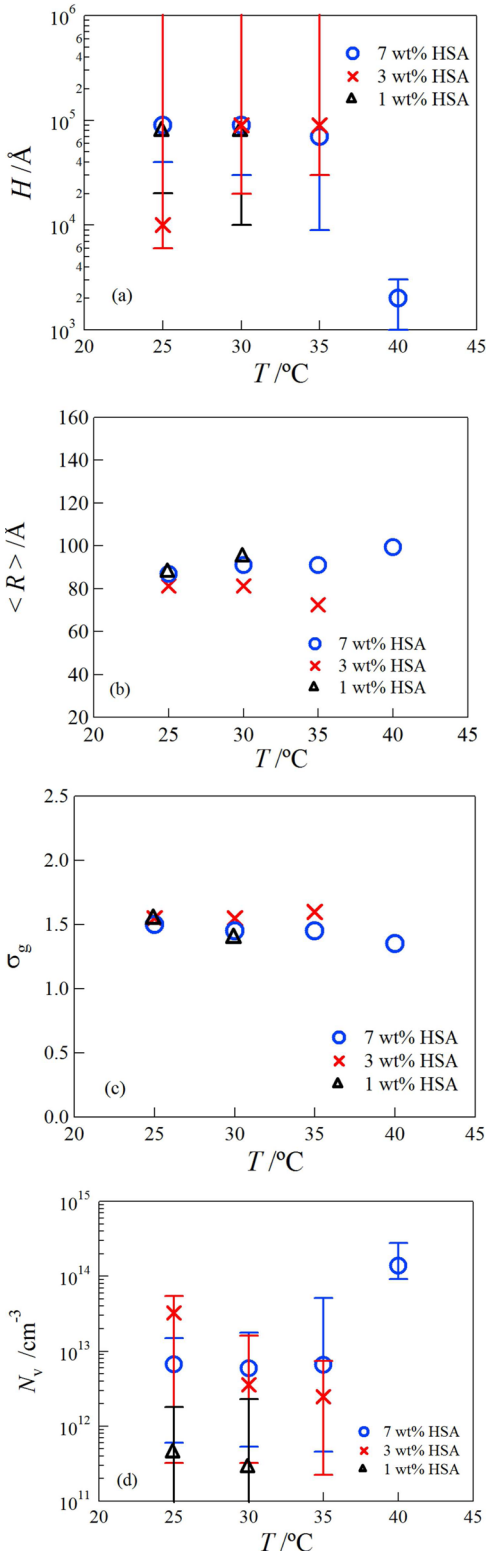

Figure 2. Temperature dependence of (a) H, (b) $\langle R \rangle$, (c) σ_g, and (d) N_v for 7, 3, and 1 wt % 12-HSA gels.

when nucleation starts to occur depends upon the temperature, that is, the induction time became shorter at the lower temperature. This result can be explained by a stronger driving force for crystallization at lower temperatures as shown by Li and co-workers.[18,19] Similar behavior was observed for turbid gel with dodecane.[20]

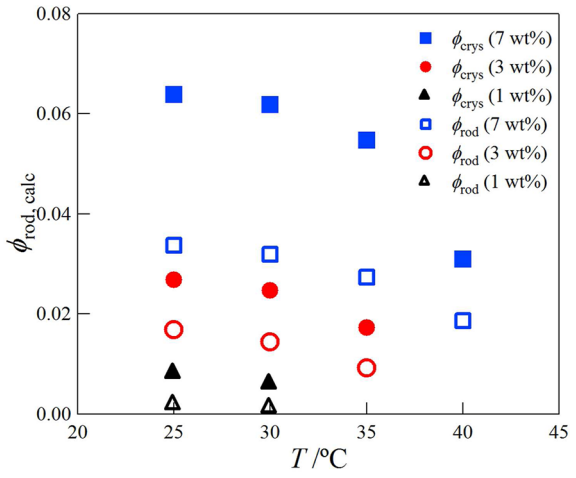

Figure 3. Temperature dependence of the volume fraction of the fiber calculated from the SANS fitting analysis (open symbols) with eq 4 and from the melting points curve (solid symbols).

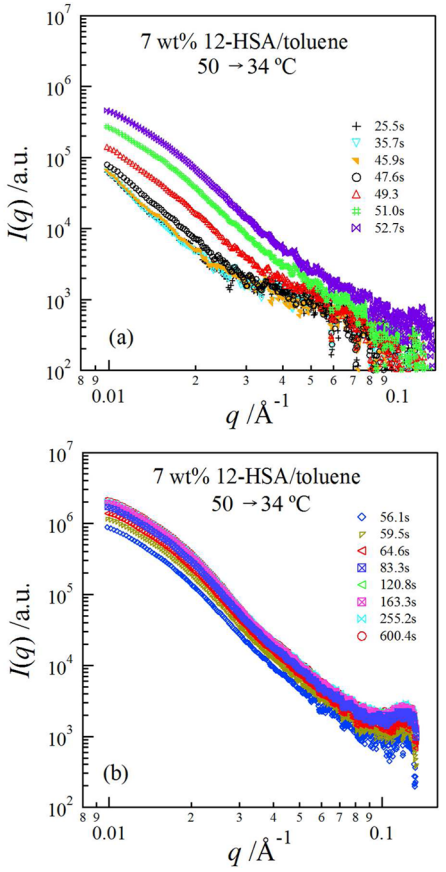

Figure 4. Time course of the SAXS profiles after the temperature jump from 50 °C (sol) to 34 °C (gel) for 7 wt % 12-HSA gel in toluene at (a) the early stage and (b) the late stage.

For sufficiently long rods, $P(q)$ is presented in the following form

$$P(q) = \frac{L\pi}{q} I_c(q) \tag{7}$$

for $2\pi/L \ll q$, where $I_c(q)$ corresponds to the scattering intensity from the cross section of the rod particles.[16,17] $I_c(q)$ can be represented by

dx.doi.org/10.1021/jp3008514 | J. Phys. Chem. B 2012, 116, 7739–7745

$$I_c(q) = A^2 \exp\left(-\frac{R_c^2 q^2}{2}\right) \quad (8)$$

for $2\pi/L \ll q \ll 2\pi/R_c$, where A and R_c are the area of the cross section and the radius of gyration of the cross section, respectively. Thus, we can estimate R_c from the linear relation between $\ln(Iq)$ versus q^2 with eqs 7 and 8. Figure 5 presents a

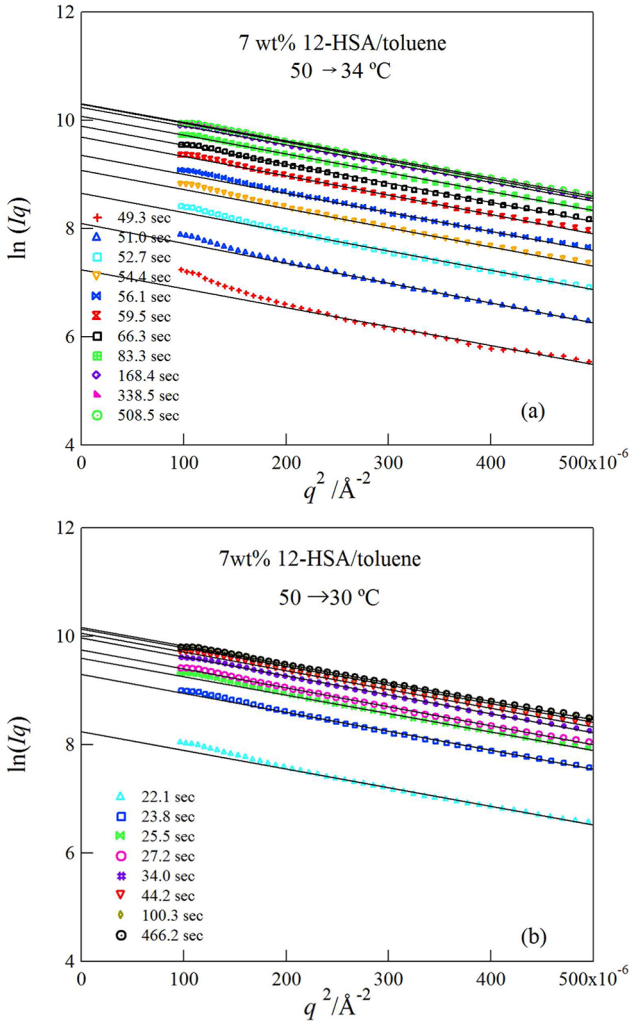

Figure 5. The plot of $\ln(Iq)$ vs q^2 for 7 wt % 12-HSA gel in toluene at (a) 34 °C and (b) 30 °C at various times.

plot of $\ln(Iq)$ versus q^2 at 34 °C (a) and at 30 °C (b) for 7 wt % 12-HSA/toluene gel at various times. The slopes of the plots at both temperatures of 34 and 30 °C did not change at various times as shown in the figures. We estimated the cross-sectional size at various times from the slope. We show the time course of R_c obtained thus in Figure 6. It is shown that the cross-sectional size of the fibers remains almost constant during the gelation process. Thus, the time-resolved SAXS experiments reveal that the fibers grow with keeping the thickness constant.

DISCUSSION

We showed in the previous section that the fiber density decreased with increasing temperature in the gel state. According to the van't Hoff equation, the solubility of the solute can be represented in the following form:[21]

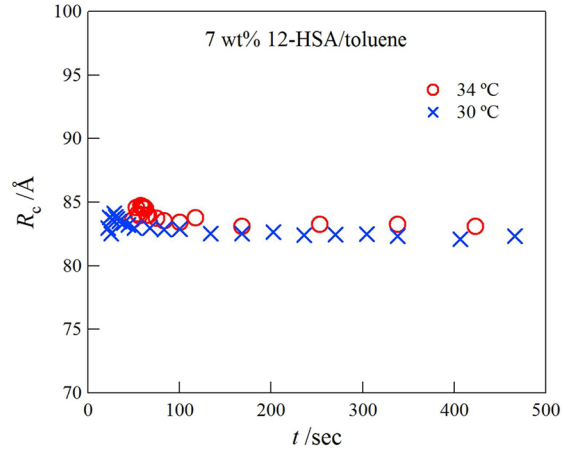

Figure 6. Time course of the radius of gyration of the fibrillar cross section during the gelation process.

$$\ln x_{eq} = -\frac{\Delta H_d}{RT} + \frac{\Delta S_d}{R} \quad (9)$$

where x_{eq}, ΔS_d, ΔH_d, and R are the equilibrium mole fraction of the solute in solution, the dissolution entropy, the dissolution enthalpy, and the gas constant, respectively. We present the plot of $\ln x_{eq}$ versus $1/T$ obtained from DSC measurements for 12-HSA/toluene mixture in Figure 7, and it shows a good linear

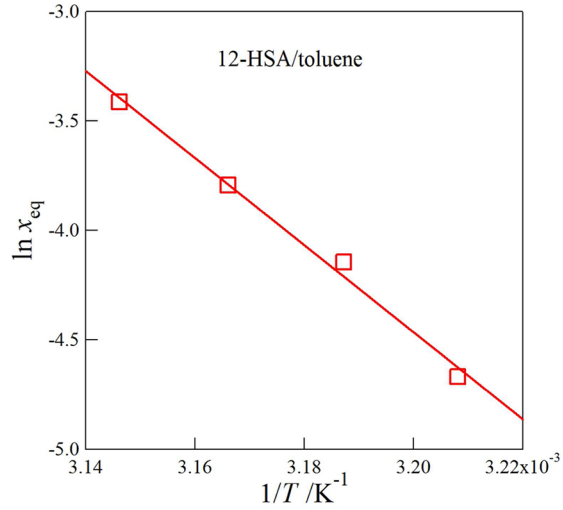

Figure 7. A plot of $\ln x_{eq}$ vs reciprocal temperature for 12-HSA gel in toluene.

relationship. From the linear relationship, ΔH_d and ΔS_d were estimated to be 165 kJ/mol and 492 J/mol, respectively. The values are close to those of n-hexatriacontane gel in silicone oil,[22] although they are in some degree larger than those of various organogels (ΔH_d = 30−160 kJ/mol).[23,24] We obtained the value of x_{eq} at the temperature of the SANS measurement from the extrapolation of the linearity and then calculated the volume fraction of the crystallites $\phi_{crys} = \Delta\phi/(1 - \phi_{eq})$ at the temperature using the lever rule, where $\Delta\phi = \phi - \phi_{eq}$ is the supersaturation and ϕ and ϕ_{eq} are the volume fraction of the gelator at preparation and the equilibrium volume fraction at the measurement temperature, respectively. The result was compared with the volume fraction of the rods obtained from the SANS analysis in Figure 3. The volume fraction of the rod

dx.doi.org/10.1021/jp3008514 | J. Phys. Chem. B 2012, 116, 7739−7745

by the SANS analysis is quite smaller than that of crystallites, although the temperature dependence is qualitatively similar to each other. Considering such discrepancy, there might be another possibility with respect to the SANS analysis. Rogers et al. indicated that 12-HSA gels in canola oil formed the crystalline network with inclusions of liquid oil by pulsed nuclear magnetic resonance.[25,26] Moreover, as mentioned above, the position of the (001) and (003) reflections for the toluene gel shifts toward slightly smaller q relative to that of the powder.[15] If not only the gelator but also the solvents are included in the fibrous phase, the result of the SANS analysis is a little different. In this case, the SANS contrast factor and the volume fraction of the fibrous phase ϕ_{rod} may be described by

$$\Delta\rho = \{x_{c,HSA}\rho_{HSA} + (1 - x_{c,HSA})\rho_{d\text{-}tol}\} - \{x_{sol,HSA}\rho_{HSA} + (1 - x_{sol,HSA})\rho_{d\text{-}tol}\} \quad (10)$$

and

$$\phi_{rod} = \frac{\phi - \phi_{s,eq}}{\phi_{c,eq} - \phi_{s,eq}} \quad (11)$$

respectively. Here, $x_{c,HSA}$, $\phi_{c,eq}$, and $\phi_{s,eq}$ represent the mole fraction, the volume fraction of HSA in the fibrous phase, and the volume fraction of HSA in the matrix phase, respectively. Assuming that eq 11 is equal to eq 6, we obtained the unknown parameters ($\phi_{c,eq}$ = 0.50−0.61 for 7 wt % gel and 0.53−0.62 for 3 wt % gel). The values of other parameters such as H, R, or σ_g do not change in comparison with the foregoing analysis using eq 4. The temperature dependence of ϕ_{rod} obtained thus is shown in Figure 8. Figure 8 indicates that the volume fraction

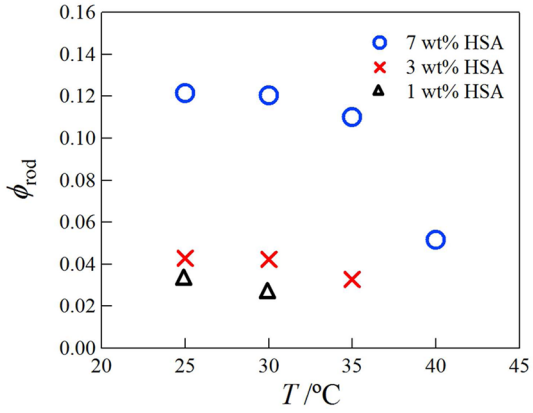

Figure 8. Temperature dependence of the volume fraction of the fiber analyzed with eqs 10 and 11.

of the fibers is larger than that of the analysis with eq 4, while it decreases with increasing temperature indicating that the fiber gradually melts with increasing temperature similar to the analysis with eq 4. In Figure 9, we present the reduced plot by the product of ϕ_{rod} and $(\Delta\rho)^2$ for the gels at various temperatures and compositions indicating that the reduced plot almost overlaps. Thus, it is shown that temperature and composition do not essentially affect the fiber structure, although they do affect the fiber density. This result may be because the pockets of solvents separating the network of fibers are larger than the length scale obtained by SANS. Therefore, contribution of interparticle scattering is sufficiently small at least in the q-scale covered in our measurements, so that the

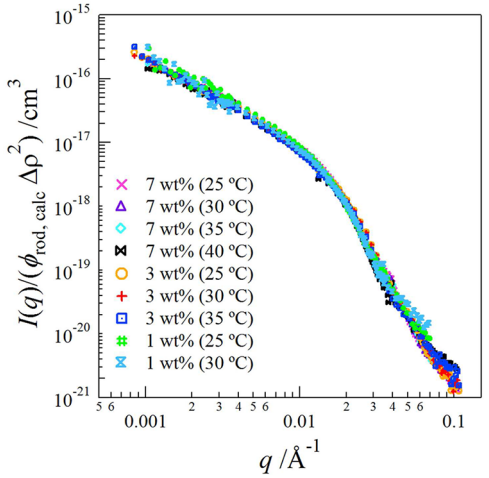

Figure 9. SANS profiles reduced by the product of the square of the SANS contrast and the volume fraction of the fibers obtained by the SANS analysis.

scattering behavior of the gel can be well reduced by the product of the volume fraction of the fibers and the square of the scattering contrast.

Next, let us discuss the gelation process investigated by the time-resolved SAXS technique. Figure 10 shows the scattering profiles reduced by the (001) peak intensity at various times. The reduced profiles can be superimposed into a single curve at both temperatures suggesting that the entire fibers possess crystalline nature. Finally, on the basis of the time-resolved SAXS result, we suppose the gelation mechanism as shown in Figure 11. After the induction period, the gelator molecules self-assemble, so that the scattering intensity increases without the reflection peak, that is, an initial structure of nucleus is formed (Figure 11a). In this regime, the gelator molecules are not arranged in a definite pattern. This might correspond to a metastable liquid-like structure as suggested by Zhang and Liu.[27] They suggested that crystallization in colloidal systems occurs via an amorphous precursor and subsequent formation of a stable crystalline structure. In the next stage, the fibers are developed via nucleation (Figure 11b) and growth. Namely, the gelator molecules collect in a pattern similar to that in the crystalline state. In this case, head-to-head contacts between carboxylic acids are formed, and the fibers grow via formation of the hydrogen bonding between hydroxy groups on the 12-carbon along the fiber axis.[11,28] The growth of the fibers proceeds with keeping the cross-sectional size constant (Figure 11c). This is probably because the rate of the crystallographic face associated with the fiber growth is so fast in comparison with that of other crystallographic faces. The further growth of the fibers leads to formation of junction points, and consequently, a self-assembled fibrillar three-dimensional network is formed (Figure 11d). Thus, the gelation completes so that the fiber growth is pinned.

CONCLUSION

We investigated the structures of 12-hydroxystearic acid solutions in the wide range from gel to sol by using small-angle neutron scattering. The crystalline fibers were formed in the gel state, and the cross-sectional size was not affected by the composition and temperature variation. The fiber density decreased with an increase of temperature. The synchrotron X-ray scattering experiments showed that the gelation process was

dx.doi.org/10.1021/jp3008514 | J. Phys. Chem. B 2012, 116, 7739−7745

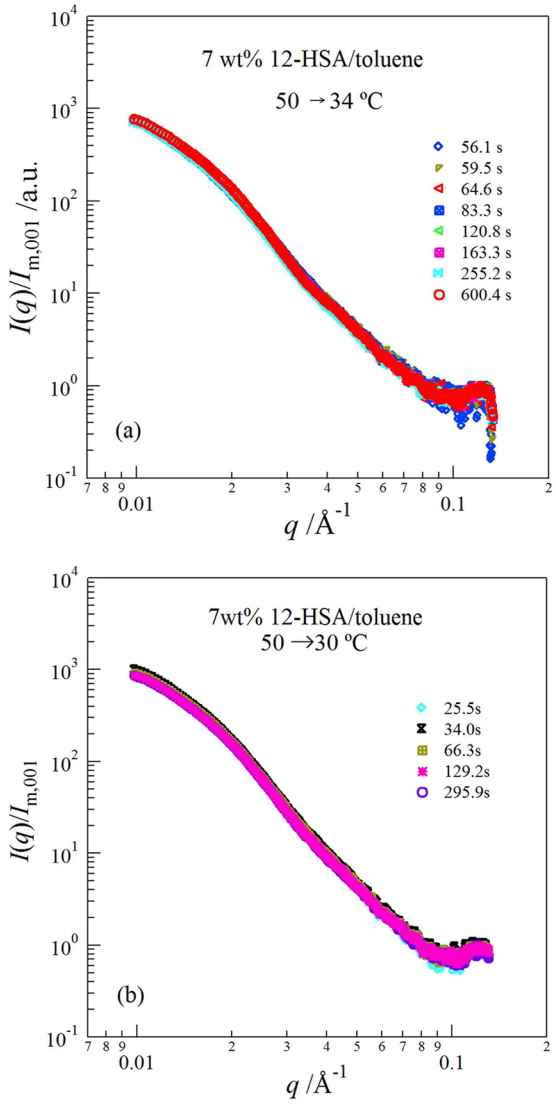

Figure 10. Scattering profiles reduced by the (001) peak intensity at various times at (a) 34 °C and (b) 30 °C.

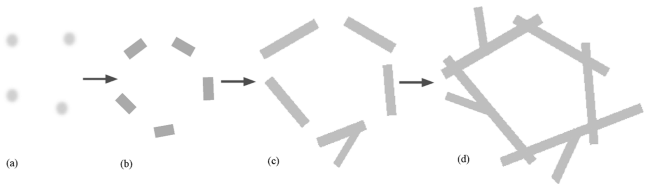

Figure 11. Schematic representation in the gelation mechanism.

developed via nucleation and growth mechanism as follows. In the early stage which corresponds to the induction period, the scattering intensity did not change with time. In the second stage, an amorphous precursor was formed before the appearance of the crystalline phase. In the next stage, a crystalline phase was created, and afterward, the crystalline fibers grew with keeping the cross-sectional size almost constant. The scattering profiles reduced by the (001) peak intensity at various times overlapped suggesting that whole fibers had a crystalline nature.

AUTHOR INFORMATION

Notes

The authors declare no competing financial interest.

REFERENCES

(1) Terech, P.; Weiss, R. G. *Chem. Rev.* **1997**, *97*, 3133−3159.
(2) Weiss, R. G.; Terech, P. *Molecular Gels Materials with Self-Assembled Fibrillar Networks*; Springer: Dordrecht, Netherlands, 2006.
(3) Raghavan, S. R. *Langmuir* **2009**, *25*, 8382−8385.
(4) Newman, S.; Krigbaum, W. R.; Carpenter, K. K. *J. Phys. Chem.* **1956**, *60*, 648−656.
(5) Boedtker, H.; Doty, P. *J. Phys. Chem.* **1954**, *58*, 968−983.
(6) Keller, A. *Faraday Discuss.* **1995**, *101*, 1−49.
(7) Okabe, S.; Ando, K.; Hanabusa, K.; Shibayama, M. *J. Polym. Sci., Part B: Polym. Phys.* **2004**, *42*, 1841−1848.
(8) Schmidt, R.; Schmutz, M.; Mathis, A.; Decher, G.; Rawiso, M.; Mesini, P. J. *Langmuir* **2002**, *18*, 7167−7173.
(9) Terech, P.; Furman, I.; Weiss, R. G. *J. Phys. Chem.* **1995**, *99*, 9558−9566.
(10) Terech, P.; Pasquier, D.; Bordas, V.; Rossat, C. *Langmuir* **2000**, *16*, 4485−4494.
(11) Terech, P.; Rodriguez, V.; Barnes, J. D.; McKenna, G. B. *Langmuir* **1994**, *10*, 3406−3418.
(12) Mallia, V. A.; George, M.; Blair, D. L.; Weiss, R. G. *Langmuir* **2009**, *25*, 8615−8625.
(13) Koizumi, S.; Iwase, H.; Suzuki, J. I.; Oku, T.; Motokawa, R.; Sasao, H.; Tanaka, H.; Yamaguchi, D.; Shimizu, H. M.; Hashimoto, T. *J. Appl. Crystallogr.* **2007**, *40*, S474−S479.
(14) Takeno, H.; Kikuchi, N.; Kondo, S.; Dobashi, T. *Trans. MRS-J.* **2007**, *32*, 835−838.
(15) Takeno, H.; Mochizuki, T.; Yoshiba, K.; Kondo, S.; Dobashi, T. *Prog. Colloid Polym. Sci.* **2009**, *136*, 47−53.
(16) Feigin, L. A.; Svergun, D. I.; Taylor, G. W. *Structure analysis by small-angle x-ray and neutron scattering*; Plenum Press: New York, 1987.
(17) Glatter, O.; Kratky, O. *Small Angle X-ray Scattering*; Academic Press: London, 1982.
(18) Li, J. L.; Liu, X. Y. *J. Phys. Chem. B* **2009**, *113*, 15467−15472.
(19) Li, J. L.; Yuan, B.; Liu, X. Y.; Xu, H. Y. *Cryst. Growth Des.* **2010**, *10*, 2699−2706.
(20) Takeno, H. et al.. To be submitted.
(21) Mullin, J. W. *Crystallization*, 4th ed.; Butterworth-Heinemann: Oxford, U.K., 2001.
(22) Abdallah, D. J.; Weiss, R. G. *Langmuir* **2000**, *16*, 352−355.
(23) Clavier, G. M.; Brugger, J. F.; Bouas-Laurent, H.; Pozzo, J. L. *J. Chem. Soc., Perk. Trans. 2* **1998**, 2527−2534.
(24) Murata, K.; Aoki, M.; Suzuki, T.; Harada, T.; Kawabata, H.; Komori, T.; Ohseto, F.; Ueda, K.; Shinkai, S. *J. Am. Chem. Soc.* **1994**, *116*, 6664−6676.
(25) Rogers, M. A.; Wright, A. J.; Marangoni, A. G. *Food Res. Int.* **2008**, *41*, 1026−1034.
(26) Rogers, M. A.; Wright, A. J.; Marangoni, A. G. *Curr. Opin. Colloid Interface Sci.* **2009**, *14*, 33−42.
(27) Zhang, T. H.; Liu, X. Y. *Angew. Chem.* **2009**, *48*, 1308−1312.
(28) Tamura, T.; Suetake, T.; Ohkubo, T.; Ohbu, K. *J. Am. Oil Chem. Soc.* **1994**, *71*, 857−861.

dx.doi.org/10.1021/jp3008514 | *J. Phys. Chem. B* 2012, 116, 7739−7745